SICE Annual Conference 2012
August 20-23, 2012, Akita University, Akita, Japan

Frequency Response Experiments of 3-D Pose Full-Tracking Visual Servoing with Eye-Vergence Hand-Eye Robot System

*Koichi Maeda[1], Mamoru Minami [2], Akira Yanou[3]
Hiroaki Matsumoto[4], Fujia Yu[5], Sen Hou[6]

Graduate School of Natural Science and Technology, Okayama University
(Tel,Fax: +81-86-251-8924;Email: {maeda, minami, yanou, matsuno, matsumoto, yu, hou}@suri.sys.okayama-u.ac.jp)

Abstract: Visual Servoing for hand-eye configuration having been presented so far seems to be vulnerable for tracking ability since it may lose a moving target. Our proposal to solve this problem is that the controller for visual servoing of the hand and the eye-vergence should be separated independently based on decoupling the motions each other. Base on this prerequisite the eye-vergence system to track target object by camera to be in view sight can have higher trackability than conventional visual servoing with fixed cameras. We have confirmed this superiority of eye-vergence system through frequency response visual servoing experiment with full 3-D pose tracking.

Keywords: Visual servoing, Eye-vergence, 3-D estimate, Frequency Response

1. INTRODUCTION

In the field of robot vision, the control method called visual servoing has attracted attention [1]-[4]. Visual servoing is a method of controlling the robot motion by installing the visual information in the feedback loop, which is obtained from the visual sensor. So, this method is expected to adapt the robot to changing or unknown environments. On the other hand, a fixed-hand-eye system has some disadvantages, making the observing ability deteriorated depending on the relative geometry of the camera and the target. Such as: the robot cannot observe the object well when it is near the cameras (Fig. 1 (a)), small intersection of the possible sight space of the two cameras (Fig. 1 (b)), and the image of the object cannot appear in the center of both cameras, so we could not get clear image information of target and its periphery, reducing the pose measurement accuracy (Fig. 1 (c)). To solve the problems above, in this paper, we propose Eye-Vergence system that gives the cameras an ability to rotate themselves to focus target at center of the images.

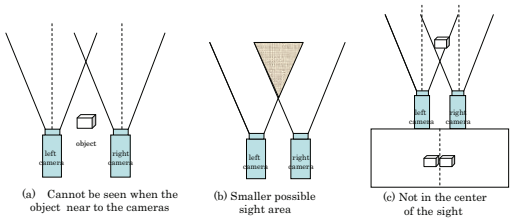

Fig. 1 Disadvantage of fix camera system

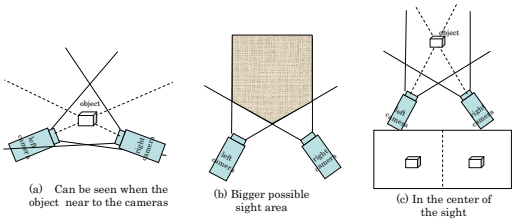

Fig. 2 Advantage of Eye-vergence system

There is no research using such rotatable hand-eye system as far as we know. Thus it is possible to change the pose of the cameras in order to observe the object better, as it is shown in Fig. 2, enhancing the measurement accuracy in trigonometric calculation and peripheral distortion of camera lens by observing target at the center of lens. Moreover, recent researches on visual servoing are limited generally in a swath of tracking an object while keeping a certain constant distance [5]-[7].

As shown in Fig.3, the proposed method includes two loops: a loop for conventional visual servoing that direct a manipulator toward a target object and an inner loop for active motion of binocular camera for accurate and broad observation of the target object. We set relatively high gain to the eye-vergence controller to put the priority to the 3D pose tracking to improve the system trackability.

we use inverse kinematics method to calculate ideal angles of links, and use this result to control joint angles to make them. It is better than control of only end effector of manipulator. We control the angles movement of the camera, to make camera move every loop. The frame frequency of stereo camera is set as 33fps in one loop. Control the angles movement can make the camera system be stable. And we also did some experiments to test trackability and stability of visual servoing.

2. 3-D OBJECT POSE ESTIMATE

In this research, we estimate an object's pose in real-time by using model-based matching (MBM) method and genetic algorism (GA). The orientation of the 3-D model and the object are representation by quaternion. Quaternion is a representation of orientation that can solve the singular posture problem of the Euler angles and Angle/axis orientation representation by choosing the angle's extent from $-\pi$ to $+\pi$. So, it is effective for making proofs of stability of visual servoing, and we have been using the quaternion in this research.

Candidates for 3-D pose of the object represented by a

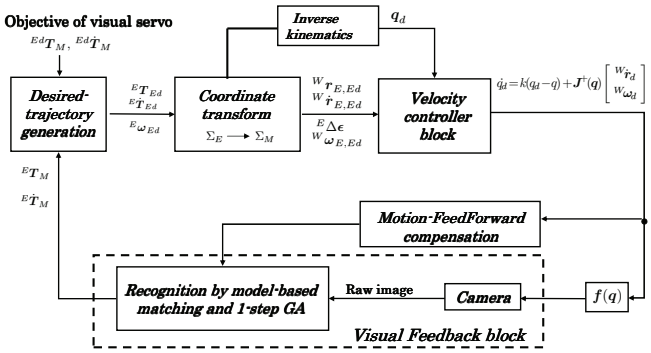

Fig. 3 Block diagram of the hand visual servoing system

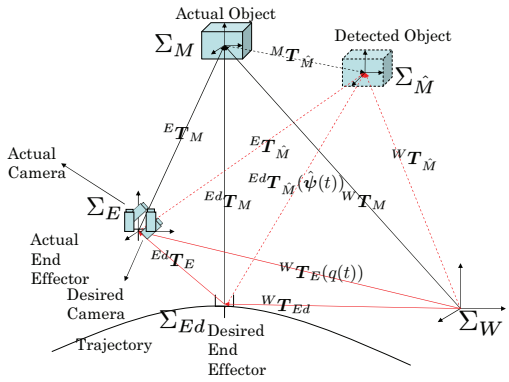

Fig. 4 Motion of the end-effector and object

quaternion are encoded as genes of GA for real-time estimation through optimization by GA. Genes evolve for optimizing the correlation function of the input image and the model as the fitness value, the pose of the object and the model in the input image is being improved and evolved into a gene representing the target's true pose.

In general, GA has not been used in real-time estimate because it generally requires some time to converge. For this problem of GA to solve, we have proposed "1-Step GA. "[8]

3. POSITION-BASED CONTROLLER

3.1 Desired-trajectory generation

In Fig. 4, the world coordinate frame is denoted by Σ_W, the target coordinate frame is denoted by Σ_M, and the desired and actual end-effector coordinate frame is denoted by Σ_{Ed}, Σ_E respectively. The desired relation between the target and the end-effector is given by Homogeneous Transformation as ${}^{Ed}\boldsymbol{T}_M$, the relation between the target and the actual end-effector is given by ${}^{E}\boldsymbol{T}_M$, then the difference between the desired end-effector pose Σ_{Ed} and the actual end-effector pose Σ_E is denoted as ${}^{E}\boldsymbol{T}_{Ed}$, which can be described by:

$$ {}^{E}\boldsymbol{T}_{Ed}(t) \quad = \quad {}^{E}\boldsymbol{T}_M(t)\,{}^{Ed}\boldsymbol{T}_M^{-1}(t) \qquad (1) $$

(1) is a general representation of hand pose tracking error that satisfies arbitrary object motion ${}^{W}\boldsymbol{T}_M(t)$ and arbitrary visual servoing objective ${}^{Ed}\boldsymbol{T}_M(t)$. The relation ${}^{E}\boldsymbol{T}_M(t)$ can be estimated by 1-step GA [5], [8], having been presented as an on-line model-based pose estimation method which will be introduced in next subsection.. Let $\Sigma_{\hat{M}}$ denote the detected object, It is natural there should always exist an error between the actual object Σ_M and the detected one $\Sigma_{\hat{M}}$. So in visual servoing, (1) will be rewritten based on $\Sigma_{\hat{M}}$ that includes the error ${}^{M}\boldsymbol{T}_{\hat{M}}$, as

$$ {}^{E}\boldsymbol{T}_{Ed}(t) \quad = \quad {}^{E}\boldsymbol{T}_{\hat{M}}(t)\,{}^{Ed}\boldsymbol{T}_{\hat{M}}^{-1}(t). \qquad (2) $$

Differentiating (2) with respect to time yields

$$ {}^{E}\dot{\boldsymbol{T}}_{Ed}(t) = {}^{E}\dot{\boldsymbol{T}}_{\hat{M}}(t)\,{}^{\hat{M}}\boldsymbol{T}_{Ed}(t) + {}^{E}\boldsymbol{T}_{\hat{M}}(t)\,{}^{\hat{M}}\dot{\boldsymbol{T}}_{Ed}(t). \qquad (3) $$

Differentiating Eq. (3) with respect to time again

$$ \begin{aligned} {}^{E}\ddot{\boldsymbol{T}}_{Ed}(t) \quad = \quad & {}^{E}\ddot{\boldsymbol{T}}_{\hat{M}}(t)\,{}^{\hat{M}}\boldsymbol{T}_{Ed}(t) + 2\,{}^{E}\dot{\boldsymbol{T}}_{\hat{M}}(t)\,{}^{\hat{M}}\dot{\boldsymbol{T}}_{Ed}(t) \\ & + {}^{E}\boldsymbol{T}_{\hat{M}}(t)\,{}^{\hat{M}}\ddot{\boldsymbol{T}}_{Ed}(t), \qquad (4) \end{aligned} $$

where ${}^{\hat{M}}\boldsymbol{T}_{Ed}$, ${}^{\hat{M}}\dot{\boldsymbol{T}}_{Ed}$, ${}^{\hat{M}}\ddot{\boldsymbol{T}}_{Ed}$ are given as the desired visual servoing objective. ${}^{E}\boldsymbol{T}_{\hat{M}}$, ${}^{E}\dot{\boldsymbol{T}}_{\hat{M}}$, ${}^{E}\ddot{\boldsymbol{T}}_{\hat{M}}$ can be observed by cameras. As shown in Fig. 4, there are two errors that we have to decrease in the visual servoing process. First one is the error between the actual object and the detected one, ${}^{M}\boldsymbol{T}_{\hat{M}}$, and the other is the error between the desired end-effector and the actual one, ${}^{E}\boldsymbol{T}_{Ed}$. In our research, the error of ${}^{M}\boldsymbol{T}_{\hat{M}}$ is decreased by pose tracking method of the "1-step GA" [8],[9], the motion feed-forward compensation [5] and the eye-vergence camera system [10], and the error of ${}^{E}\boldsymbol{T}_{Ed}$ depends on the performances of the hand visual servoing controller, being explained next.

3.2 On-line Pose Tracking "1-step GA"

For real-time visual control purposes, we employ GA in a way that we denoted as "1-Step GA"[8] evolution in which the GA evolutional iteration is applied one time to the newly input image. While using the elitist model of the GA, the position/orientation of a target can be detect in every new image by that of the searching model given by the best individual in the population. This feature happens to be favorable for real-time visual recognition. We output the current best individual of the GA in every newly input image, and use it as real-time recognition result.

However, as the searching space extending to 3D, the time of each GA process will become longer since the parameters is increased to six. So the dynamics of recognition will become worse. The proposed MFF recognition method [5] can help us conduct such a task since it can predict the motion of the target seeing from the cameras based on the motion of the robot. So when it got converged, GA group will move together with the moving of the target in the image, never loose it even under a high-speed moving of robot manipulator.

3.3 Hand & Eye Visual Servoing Controller

3.3.1 Hand Visual Servoing Controller

The block diagram of our proposed hand & eye-vergence visual servoing controller is shown in Fig. 3. The hand-visual servoing is the outer loop. A detailed block diagram of hand visual servoing control is depicted in Fig.3. Based on the above analysis of the desired-trajectory generation, the desired hand velocity ${}^{W}\dot{\boldsymbol{r}}_d$ is

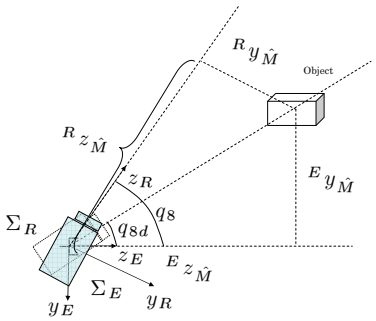

Fig. 5 Calculation of tilt angle

calculated as,

$$^{W}\dot{\boldsymbol{r}}_d = \boldsymbol{K}_{P_p}{}^{W}\boldsymbol{r}_{E,Ed} + \boldsymbol{K}_{V_p}{}^{W}\dot{\boldsymbol{r}}_{E,Ed}, \quad (5)$$

where $^{W}\boldsymbol{r}_{E,Ed}$, $^{W}\dot{\boldsymbol{r}}_{E,Ed}$ can be calculated from $^{E}\boldsymbol{T}_{Ed}$ and $^{E}\dot{\boldsymbol{T}}_{Ed}$. $\boldsymbol{K}_{P_p}$ and $\boldsymbol{K}_{V_p}$ are positive definite matrix to determine PD gain.

The desired hand angular velocity $^{W}\boldsymbol{\omega}_d$ is calculated as,

$$^{W}\boldsymbol{\omega}_d = \boldsymbol{K}_{P_o}{}^{W}\boldsymbol{R}_E{}^{E}\Delta\boldsymbol{\epsilon} + \boldsymbol{K}_{V_o}{}^{W}\boldsymbol{\omega}_{E,Ed}, \quad (6)$$

where $^{E}\Delta\boldsymbol{\epsilon}$ is a quaternion error [8] calculated from the pose tracking result, and $^{W}\boldsymbol{\omega}_{E,Ed}$ can be computed by transforming the base coordinates of $^{E}\boldsymbol{T}_{Ed}$ and $^{E}\dot{\boldsymbol{T}}_{Ed}$ from Σ_E to Σ_W. Also, $\boldsymbol{K}_{P_o}$ and $\boldsymbol{K}_{V_o}$ are suitable feedback matrix gains. We define the desired hand pose as $^{W}\boldsymbol{\psi}_d^T = [^{W}\boldsymbol{r}_d^T, {}^{W}\boldsymbol{\epsilon}_d^T]^T$

The desired joint variable $\boldsymbol{q}_d$ and $\dot{\boldsymbol{q}}_d$ is obtained by

$$\boldsymbol{q}_d = \boldsymbol{f}^{-1}(^{W}\boldsymbol{\psi}_d^T) \quad (7)$$

$$\dot{\boldsymbol{q}}_d = \boldsymbol{J}^{+}(\boldsymbol{q}) \begin{bmatrix} ^{W}\dot{\boldsymbol{r}}_d \\ ^{W}\boldsymbol{\omega}_d \end{bmatrix} \quad (8)$$

where $\boldsymbol{f}^{-1}(^{W}\boldsymbol{\psi}_d^T)$ is the inverse kinemetic function and $\boldsymbol{J}^{+}(\boldsymbol{q})$ is the pseudoinverse matrix of $\boldsymbol{J}(\boldsymbol{q})$, and $\boldsymbol{J}^{+}(\boldsymbol{q}) = \boldsymbol{J}^{T}(\boldsymbol{J}\boldsymbol{J}^{T})^{-1}$.

The Mitsubishi PA-10 robot arm is a 7 links manipulator, and the end-effector has 6-DoF, so it has a redundance. In the research before, we only calculated the position of the manipulator's end-effector, but not considering the joint angles through the position of the manipulator's end-effector. For one end-effector pose, there may exist infinite kinds of shapes, which will make the system dangerous. In this report, we made q_1 is 0, and used the inverse kinematics to calculate all joint angles. It can solve the redundancy problem. Meanwhile we took a controller to make the joint of angles approximately as the desired joint angles. So we defined the formula of the desired joint angles in the new controller as

$$\dot{\boldsymbol{q}}_d = \boldsymbol{k}_p(\boldsymbol{q}_d - \boldsymbol{q}) + \boldsymbol{J}^{+}(\boldsymbol{q}) \begin{bmatrix} ^{W}\dot{\boldsymbol{r}}_d \\ ^{W}\boldsymbol{\omega}_d \end{bmatrix} \quad (9)$$

where $\boldsymbol{k}_p$ is P positive gain.

The hardware control system of the velocity-based servo system of PA10 is expressed as

$$\boldsymbol{\tau} = \boldsymbol{K}_{SP}(\boldsymbol{q}_d - \boldsymbol{q}) + \boldsymbol{K}_{SD}(\dot{\boldsymbol{q}}_d - \dot{\boldsymbol{q}}) \quad (10)$$

where $\boldsymbol{K}_{SP}$ and $\boldsymbol{K}_{SD}$ are symmetric positive definite matrices to determine PD gain.

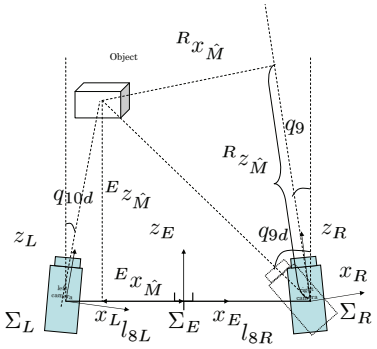

Fig. 6 Calculation of pan angles

3.3.2 Eye-vergence Visual Servoing Controller

The eye-vergence visual servoing is the inner loop of the visual servoing system shown in Fig. 3. In this paper, we use two pan-tilt cameras for eye-vergence visual servoing. Here, the positions of cameras are supposed to be fixed on the end-effector. For camera system, q_8 is tilt angle, q_9 and q_{10} are pan angles, and q_8 is common for both cameras. As it is shown in Fig. 5 and Fig. 6, $^{E}x_{\hat{M}}$, $^{E}y_{\hat{M}}$, $^{E}z_{\hat{M}}$ express position of the detected object in the end-effector coordinate. The desired angle of the camera joints are calculated by:

$$q_{8d} = atan2(^{E}y_{\hat{M}}, {}^{E}z_{\hat{M}}) \quad (11)$$

$$q_{9d} = atan2(-l_{8R} + {}^{E}x_{\hat{M}}, {}^{E}z_{\hat{M}}) \quad (12)$$

$$q_{10d} = atan2(l_{8L} + {}^{E}x_{\hat{M}}, {}^{E}z_{\hat{M}}) \quad (13)$$

where $l_{8L} = l_{8R} = 120[mm]$ that is the camera location. We set the center line of the camera as the z axis of each camera coordinate, so the object will be in the center of the sight of the right camera when $^{R}x_{\hat{M}} = 0$ and $^{R}y_{\hat{M}} = 0$, $^{R}x_{\hat{M}}$, $^{R}y_{\hat{M}}$, $^{R}z_{\hat{M}}$ express the position of the detected object in the right camera coordinate. The controller of eye-visual servoing is given by

$$\dot{q}_8 = K_P(q_{8d} - q_8) + K_D(\dot{q}_{8d} - \dot{q}_8) \quad (14)$$

$$\dot{q}_9 = K_P(q_{9d} - q_9) + K_D(\dot{q}_{9d} - \dot{q}_9) \quad (15)$$

$$\dot{q}_{10} = K_P(q_{10d} - q_{10}) + K_D(\dot{q}_{10d} - \dot{q}_{10}) \quad (16)$$

where K_P, K_D are positive control gain.

Because the motion of camera motor is an open loop, we can only make it rotate a certain degree without getting the actual angle during the rotation, which make us cannot get the accurate camera angle. So the desired camera angles are input in every 33ms, and the input is limited to a certain value.

4. EXPERIMENT OF HAND & EYE-VERGENCE VISUAL SERVOING

4.1 Experimental system

To verify the effectiveness of the hand & eye visual servoing system through real robot, we used a robot, Mitsubishi PA-10 robot arm that has a 7-DoF robot arm manufactured by Mitsubishi Heavy Industries. Two rotatable cameras mounted on the end-effector are FCB-1X11A manufactured by Sony Industries. The frame frequency of stereo cameras is set as 30fps. The image processing

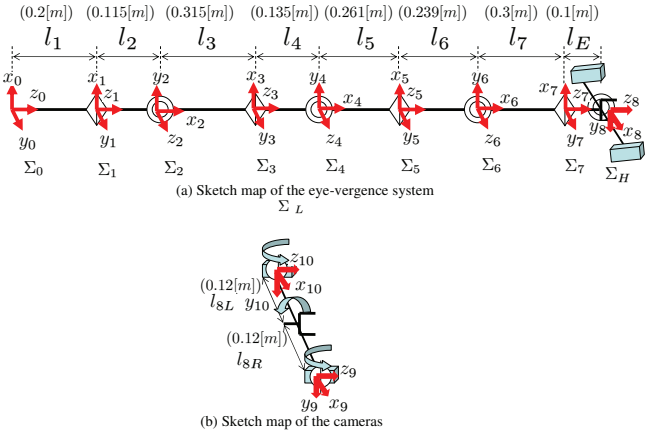

(a) Sketch map of the eye-vergence system Σ_L

(b) Sketch map of the cameras

Fig. 7 Frame structure of manipulator

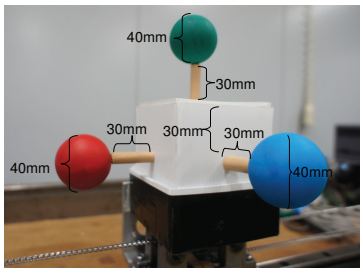

Fig. 8 3D marker

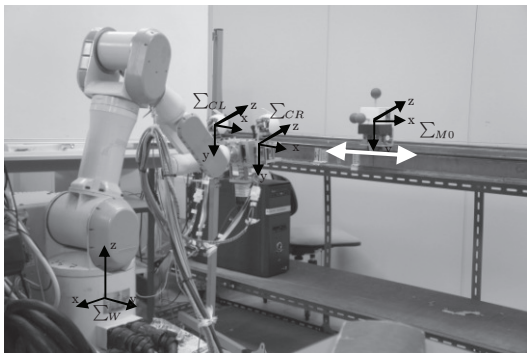

Fig. 9 Object and the visual-servoing system

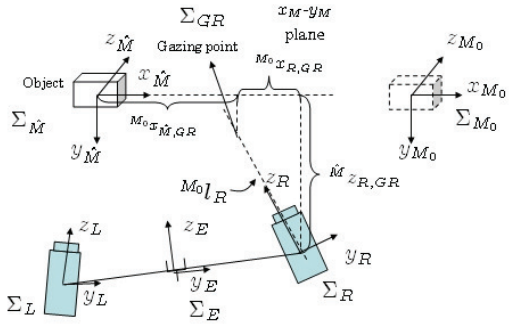

Fig. 10 Cameras' and End Effector's gazing point

board, CT-3001, receiving the image from the CCD camera is connected to the DELL WORKSTATION PWS650 (CPU: Xeon, 2.00 GHz) host computer. The structure of the manipulator and the cameras are shown in Fig. 7 (a) and (b).

The 3D marker as used for the target object in the experiment composes a red ball, a green ball and a blue ball, whose dimension is shown in Fig. 8. The coordinate of the target object and the manipulator in experiment are shown in Fig. 9, the white arrow under the object express the move direction of it.

In order to check the visual servoing system, first, we did an experiment in which true object's, x, y, z, ε_1, ε_2, ε_3, are assumed to be given to servoing controller. Then we did 3 groups of experiments of frequency response. In these experiments, we made x-position, 3-Dof position, and 6-Dof position/orientation are recognized by the cameras respectively. For every group, we set ω=0.314, ω=0.628, and ω=1.256 separately, which are angular velocities of the object.

4.2 Experiment condition

The initial hand pose is defined as Σ_{E_0}, and the initial object pose is defined as Σ_{M_0}. The homogeneous transformation matrix from Σ_W to Σ_{E_0} and from Σ_W to Σ_{M_0} are:

$$ {}^{W}\boldsymbol{T}_{E_0} = \begin{bmatrix} 0 & 0 & -1 & -690[mm] \\ 1 & 0 & 0 & -150[mm] \\ 0 & -1 & 0 & 465[mm] \\ 0 & 0 & 0 & 1 \end{bmatrix} \quad (17) $$

$$ {}^{W}\boldsymbol{T}_{M_0} = \begin{bmatrix} 0 & 0 & -1 & -1235[mm] \\ 1 & 0 & 0 & -150[mm] \\ 0 & -1 & 0 & 555[mm] \\ 0 & 0 & 0 & 1 \end{bmatrix} \quad (18) $$

The target object move according to the following time function

$$ {}^{W}\boldsymbol{T}_{M} = \begin{bmatrix} 0 & 0 & -1 & -1235[mm] \\ 1 & 0 & 0 & -150\cos(\omega t)[mm] \\ 0 & -1 & 0 & 555[mm] \\ 0 & 0 & 0 & 1 \end{bmatrix} \quad (19) $$

The relation between the object and the desired end-effector is set as:

$$ {}^{Ed}\boldsymbol{\psi}_M = [0, -90[mm], 545[mm], 0, 0, 0] \quad (20) $$

4.3 Definition of trackability

Here, to compare the trackability of the eye-vergence system and fixed camera system, we define a concept of gazing point. As it is shown in Fig. 10 the intersection of the gazing line of right camera and the x_{M_0}-y_{M_0} plane is defined as the gazing point. The relative relation between Σ_{M_0} and Σ_R is given by Homogeneous Transformation as ${}^{M_0}\boldsymbol{T}_R$, ${}^{M_0}\boldsymbol{T}_R$ conclude the rotation matrix ${}^{M_0}\boldsymbol{R}_R$ and the position vector ${}^{M_0}\boldsymbol{p}_R$, and the rotation matrix ${}^{M_0}\boldsymbol{R}_R$ can be written as $[{}^{M_0}\boldsymbol{x}_R, {}^{M_0}\boldsymbol{y}_R, {}^{M_0}\boldsymbol{z}_R]$. The direction of ${}^{M_0}\boldsymbol{l}_R$ in Fig. 10 is same to the direction of z_R, and ${}^{M_0}\boldsymbol{l}_R$ can be expressed as:

$$ {}^{M_0}\boldsymbol{l}_R = {}^{M_0}\boldsymbol{p}_R + k_R {}^{M_0}\boldsymbol{z}_R \quad (21) $$

here k_R is a scalar variable. The gazing point of the right camera expressed in Σ_{M_0} is ${}^{M_0}\boldsymbol{p}_{GR} = [{}^{M_0}x_{GR}, {}^{M_0}y_{GR}, 0]^T$. For ${}^{M_0}\boldsymbol{l}_R = {}^{M_0}\boldsymbol{p}_{GR}$ in z direction, $({}^{M_0}\boldsymbol{p}_R)_z + k_R({}^{M_0}\boldsymbol{z}_R)_z = 0$. And usually $({}^{M_0}\boldsymbol{z}_R)_z \neq 0$, k_R can be calculated by $k_R = -({}^{M_0}\boldsymbol{p}_R)_z/({}^{M_0}\boldsymbol{z}_R)_z$, and the x, y coordinate of the gazing point in Σ_{M_0} can be calcated by:

$$ {}^{M_0}x_{GR} = ({}^{M_0}\boldsymbol{p}_R)_x + k_R({}^{M_0}\boldsymbol{z}_R)_x \quad (22) $$

$$ {}^{M_0}y_{GR} = ({}^{M_0}\boldsymbol{p}_R)_y + k_R({}^{M_0}\boldsymbol{z}_R)_y \quad (23) $$

The target object's motion is given by (19), because the motion of the target object M is parallel to the $\boldsymbol{x}_{M_0}$, we take ${}^{M_0}x_M(t)$ as the input, and the gazing point of the right camera ${}^{M_0}x_{GR}(t)$ as the response. And define the concept of trackability by the frequency response of ${}^{M_0}x_{GR}(t)$, the trackability of the left camera can be defined in the same way.

4.4 Experiment Results

In Fig. 11, we show the results of our experiments which gave the position and orientation of the object to the robot directly. We change the ω=0.314, to ω=0.628, and ω=1.256, and get the data of the gazing point of the cameras in the eye-vergence system and the gazing point of the end-effector of the fixed camera system separately (a), (b) and (c). We did each experiment for 40s at every ω above, and got the average delay time and the amplitude to draw the frequence response curve. The amplitude-frequence curve and the delay frequency curve are shown in Fig.11 (d) and (e). Here, for the fixed camera $A = {}^{M_0}x_M(t)$, $B = {}^{M_0}x_{GE}(t)$. For the right camera of Eye-Vergence system $A = {}^{M_0}x_M(t)$, $B = {}^{M_0}x_{GR}(t)$, for the left camera $A = {}^{M_0}x_M(t)$, $B = {}^{M_0}x_{GL}(t)$. In this two figures the abscissa axes are ω.From (d), the curve of the fixed camera system is always below the curves of the cameras, we can see that the amplitude of the eye-vergence system is more closed to the target object than the fixed camera system. And from (e) the the curve of the fixed camera system is also below the curves of the cameras, which means that delay of the fixed camera system is bigger than the eye-vergence system. We made x-position, 3-Dof position, and 6-Dof position/orientation are recognized by the cameras respectively, and take the results in Fig.12, Fig.13, and Fig.14. From each of the figures we can see that the eye-vergence system has smaller delay phase which means it will observe the object better.

5. CONCLUSION

We did some experiments to evaluate the observation ability on a moving object of visual servoing system. To evaluate dynamical merits and kinematic merits of eye-vergence visual servoing system, we have analyzed trackability, amplitude-frequency and phase-frequency curves of the cameras of the eye-vergence system and the fixed camera system under moving object with different angular velocity, and have got the conclusion that the trackability and stability of the eye-vergence system is better than that of the fixed-camera system.

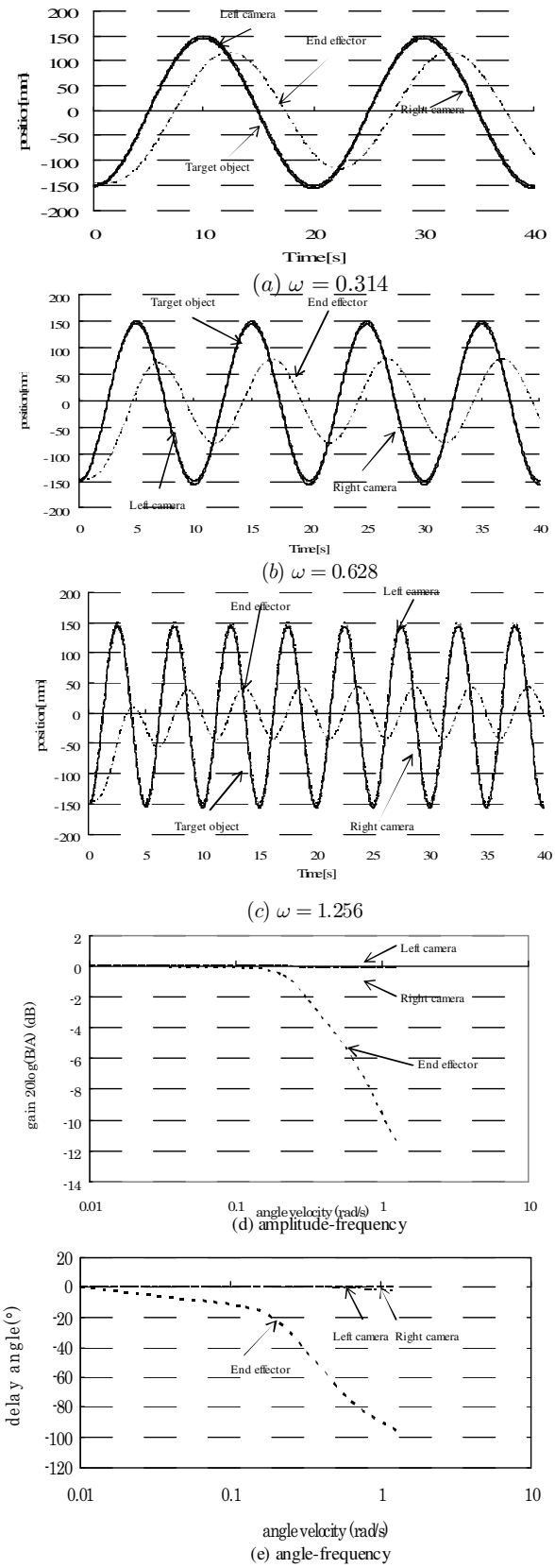

Fig. 11 True object's pose is directly given to the system, which can cancel the recognition error, so in this figure we can see only the dynamic error, and the camera can track the object much better than the end-effector

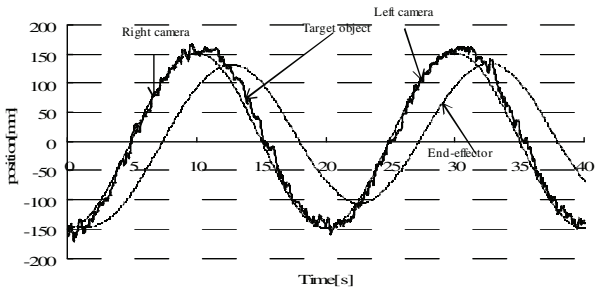

$(a)\ \omega = 0.314$

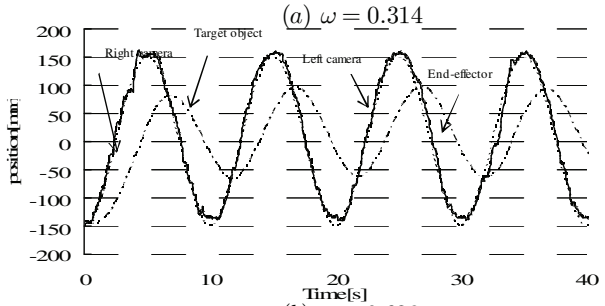

$(b)\ \omega = 0.628$

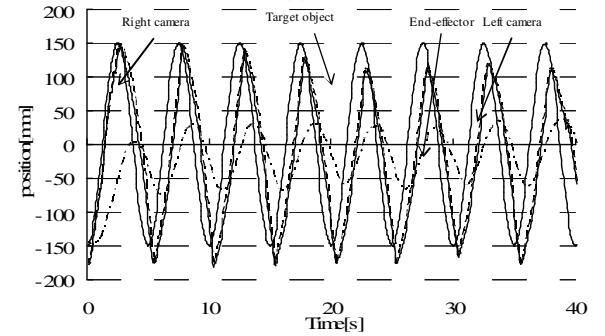

$(c)\ \omega = 1.256$

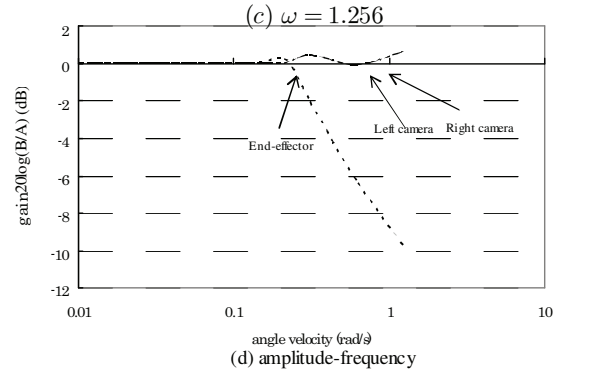

(d) amplitude-frequency

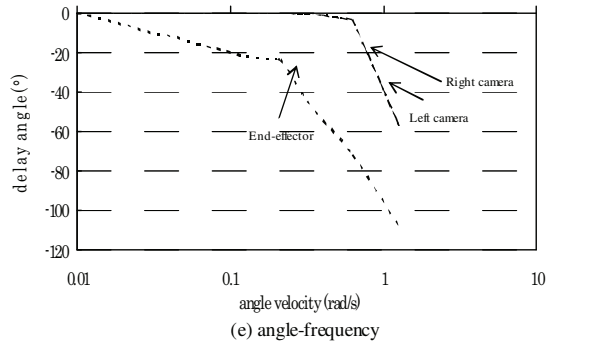

(e) angle-frequency

Fig. 12 The object's pose, y, z, $\varepsilon 1$, $\varepsilon 2$, $\varepsilon 3$, are assumed to be given to servoing controller

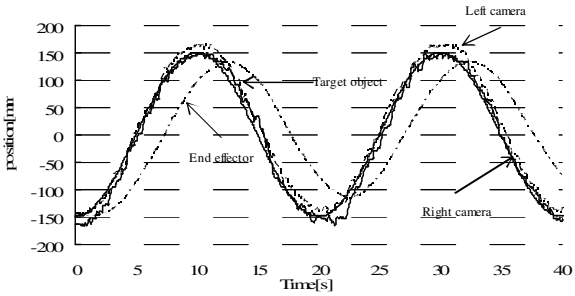

$(a)\ \omega = 0.314$

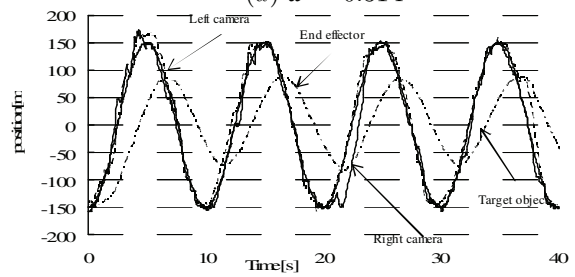

$(b)\ \omega = 0.628$

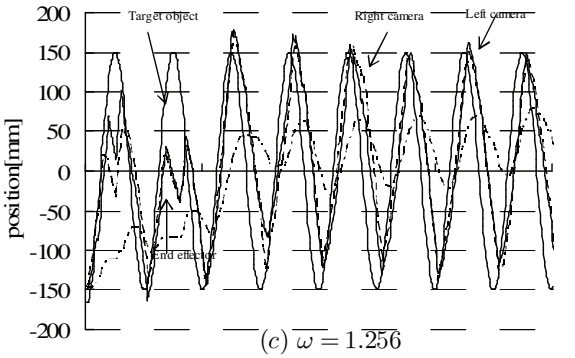

$(c)\ \omega = 1.256$

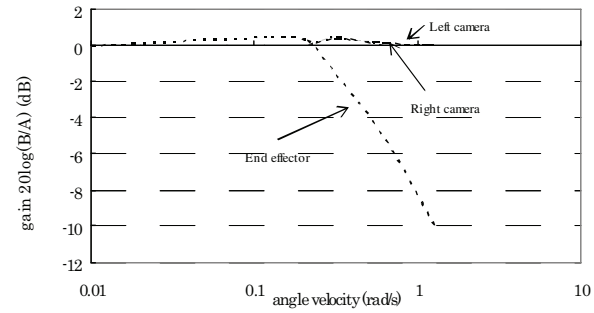

(d) amplitude-frequency

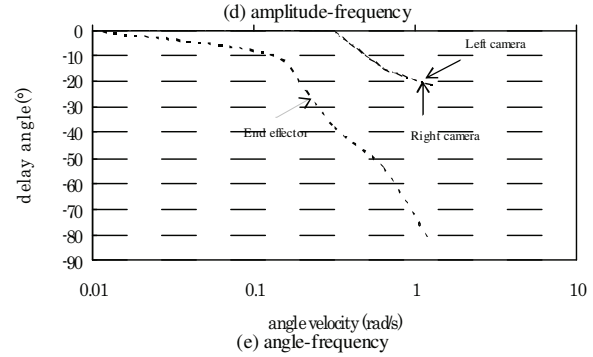

(e) angle-frequency

Fig. 13 The object's pose, $\varepsilon 1$, $\varepsilon 2$, $\varepsilon 3$, are assumed to be given to servoing controller

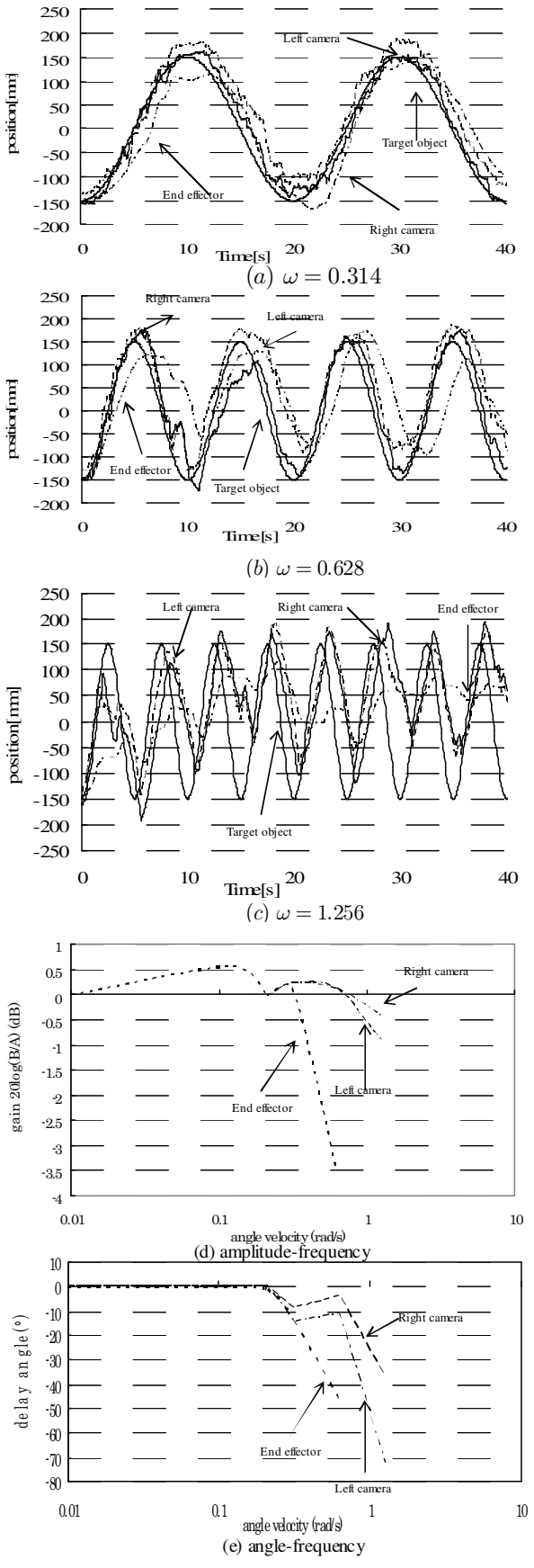

Fig. 14 The object's pose x, y, z, $\varepsilon 1$, $\varepsilon 2$, $\varepsilon 3$, are recognized by camera

REFERENCES

[1] S.Hutchinson, G.Hager, and P.Corke, "A Tutorial on Visual Servo Control", IEEE Trans. on Robotics and Automation, vol. 12, no. 5, pp. 651-670, 1996.

[2] P.Y.Oh, and P.K.Allen, "Visual Servoing by Partitioning Degrees of Freedom", IEEE Trans. on Robotics and Automation, vol. 17, no. 1, pp. 1-17, 2001.

[3] E.Malis, F.Chaumentte and S.Boudet, "2-1/2-D Visual Servoing", IEEE Trans. on Robotics and Automation, vol. 15, no. 2, pp. 238-250, 1999.

[4] P.K.Allen, A.Timchenko, B.Yoshimi, and P.Michelman, "Automated Tracking and Grasping of a Moving object with a Robotic Hand-Eye System", IEEE Trans. on Robotics and Automation, vol. 9, no. 2, pp. 152-165, 1993.

[5] W. Song, M. Minami, Y. Mae and S. Aoyagi, "Online Evolutionary Head Pose Measurement by Feedforward Stereo Model Matching", IEEE Int. Conf. on Robotics and Automation (ICRA), pp.4394-4400, 2007.

[6] Omar Tahri and Francois Chaumette, "Point-Based and Region-Based Image Moments for Visual Servoing of Planar Objects", IEEE Tran. on Robotics, vol. 21, no. 6, Dec 2005.

[7] Tarek Hamel and Robert Mahony, "Visual Servoing of an Under-Actuated Dynamic Rigid-Body System: An Image-Based Approach", IEEE Trans. on Robotics and Automation, VOL. 18, NO. 2, APRIL 2002.

[8] W. Song, M. Minami, S. Aoyagi, "On-line Stable Evolutionary Recognition Based on Unit Quaternion Representation by Motion-Feedforward Compensation", International Journal of Intelligent Computing in Medical Sciences and Image Processing (IC-MED) Vol. 2, No. 2, Page 127-139 (2007).

[9] M.Minami, W.Song, "Hand-eye-motion Invariant Pose Estimation with On-line 1-step GA -3D Pose Tracking Accuracy Evaluation in Dynamic Hand-eye Oscillation", Journal of Robotics and Mechatronics, Vol.21, No.6, pp.709-719 (2009.12)

[10] Wei. Song, M. Minami, Fujia Yu, Yanan Zhang and Akira Yanou "3-D Hand & Eye-Vergence Approaching Visual Servoing with Lyapunouv-Stable Pose Tracking ", IEEE Int. Conf. on Robotics and Automation (ICRA), pp.11, 2011.